Synergistic effects of the electric field induced by imidazolium rotation and hydrogen bonding in electrocatalysis of CO_2

Oguz Kagan Coskun, Zeynep Bagbudar, Vaishali Khokhar, Saudagar Dongare, Robert E. Warburton, Burcu Gurkan*

Department of Chemical and Biomolecular Engineering, Case Western Reserve University, Cleveland, Ohio, USA, 44106

***E-mail:** beg23@case.edu

Abstract

The roles of the ionic liquid, 1-ethyl-3-methylimidazolium tetrafluoroborate ([EMIM][BF_4]), and water in controlling the mechanism, energetics, and electrocatalytic activity of CO_2 reduction to CO on silver in non-aqueous electrolytes were investigated. The first electron transfer occurs to CO_2 at reduced overpotentials when it is trapped between the planes of $[EMIM]^+$ ring and electrode surface due to cation re-orientation as determined from voltammetry, in-situ surface enhanced Raman spectroscopy, and density functional theory calculations. Within this interface, water up to 0.5 M does not induce significant faradaic activity, opposing the notion of it as a free proton source. Instead, water acts as a hydrogen bond donor and the proton is sourced from $[EMIM]^+$. Furthermore, this study demonstrates that alcohols with varying acidity tune the hydrogen bonding network in the interfacial microenvironment to lower the energetics required for CO_2 reduction. The hydrogen bonding suppresses the formation of inactive carboxylate species, thus preserving the catalytic activity of $[EMIM]^+$. The ability to tune hydrogen bonding network opens new avenues for advancing IL-mediated electrocatalytic reactions in non-aqueous electrolytes.

INTRODUCTION

Realization of electrochemical reduction of carbon dioxide (CO_2RR) to convert the CO_2 greenhouse gas into fuels and chemicals depends on the discovery of efficient catalysts and electrolytes with high CO_2 solubilities. CO_2RR on heterogeneous electrocatalysts is an inner-sphere process[1] that unfolds within the Helmholtz plane[2] at the electrode-electrolyte interface that is enriched in cations due to the negative polarization of the electrode; which in turn govern the reactivity and selectivity in CO_2RR. [3, 4] The CO_2 reduction mechanism involves the formation of the anion radical intermediate ($CO_2^{\bullet-}$)[5, 6] where a high overpotential is needed. Notably, the imidazolium based ionic liquids (ILs) with high CO_2 solubility, in particular 1-ethyl-3-methyl-imidazolium tetrafluoroborate ([EMIM][BF_4]), have been shown to lower the energy barrier for CO_2 to CO conversion.[7] $[EMIM]^+$ is reported to exhibit a unique ability to cover the entire electrode surface (e.g., Ag), even in diluted conditions.[8] Further, $[EMIM]^+$ undergoes orientation changes from tilted to a parallel configuration with respect to the electrode surface with increasing negative polarization.[9-13] Separately, the electric field effects of [EMIM][BF_4] on Ag were probed indirectly through the change in Stark shift of CO by sum frequency generation spectroscopy.[14] A 2-fold increase in the Stark shift was observed and attributed to doubling of the electric field strength. The induced electric field effects were associated to the stabilization of $CO_2^{\bullet-}$ by a density functional theory (DFT) study, thus rationalizing the lowered overpotentials in CO_2RR by cations (e.g., K^+ and $[EMIM]^+$).[15] Even though this understanding led to the modification of the screening and electric field effects through the adjustment of the IL concentration where the existence of an optimal range to influence kinetics was confirmed,[16] a physical model of the interfacial evolution with $[EMIM]^+$, the induced electric field effects, and interacting species at the interface is still not

complete. Such a complete model is needed to rationalize the observed thermodynamics and kinetics of IL mediated CO_2RR and reveal the mechanism.

Besides the modification of the electric field, the imidazolium cations are discussed to complex with CO_2 to form carboxylate adducts, as evidenced by spectroscopy, then mediate the electron transfer reaction.[7, 17, 18] It was proposed that the imidazolium cation radical has to form first before the carboxylate,[19, 20] and that the imidazolium radical serves as a catalyst.[21] An alternative pathway considers the initial electron transfer to CO_2, followed by an interaction between C_2 position and $CO_2^{\bullet-}$. [22] When the imidazolium cation is involved, the presence of $CO_2^{\bullet-}$ was confirmed using surface-enhanced infrared absorption spectroscopy, facilitating its prolonged presence at the interface through stabilization by the imidazolium.[23] The depletion of CO_2 at the interface was further observed, by employing attenuated total reflection spectroscopy, at potentials more negative than the onset potential observed by transient voltammetry studies, pointing to the slow reaction kinetics following the initial electron transfer. [24] Subsequently, an isomerization step transfers the C_2-H to COO^- moiety to form EMIM-COOH. The involvement of C_2-H in CO_2 conversion to CO was also probed through the hydrogen-deuterium exchange between $[EMIM]^+$ and D_2O where a more negative onset potential with deuterated cations $[EMIM\text{-}D]^+$ compared to conventional cations $[EMIM\text{-}H]^+$ was measured.[25] However, harvesting C_2-H from the imidazolium results in an unstable imidazolium carbene product, as also evidenced through electron paramagnetic resonance spectroscopy[26] and computational studies.[27] These carbenes are shown to preferentially bind to the Ag electrode surface, occupying its active sites.[28] Furthermore, upon formation, imidazolium carbenes can react with dissolved CO_2 to generate carboxylate adducts, which are reported to be a side product and inactive for the electrochemical conversion cycle.[29] However, in the presence of water, rapid protonation of the carboxylate to form EMIM-

COOH has been observed,[30, 31] thereby activating the imidazolium carboxylate and further regenerating the imidazolium cation, thus recovering catalytic activity of the imidazolium after water addition.[32]

Conventionally, the role of water is perceived as that of the proton source in nonaqueous electrolytes. For water to fulfill this role, it must undergo reduction to liberate free protons at the electrode surface, which can then participate in CO_2 conversion reaction. The addition of water to nonaqueous IL electrolytes typically increases CO_2 reduction reaction rates due to the availability of free protons.[33, 34] However, a recent infrared reflection-absorption spectroscopy study[35] reported no significant changes in water-related bands during catalysis, suggesting that water is not consumed as a reactant in CO_2 reduction. Rather, they reported the formation of EMIM-COOH and a CO_2 reduction onset potential that depends on water concentration. This suggests that while the water facilitates the formation of EMIM-COOH, it is not consumed in the process. Separately, other studies have shown that water bridges the IL cation and the surface adsorbed species (e.g., *COOH),[36, 37] through hydrogen bonding to both, instead of IL interacting directly with the surface species.[38] This hydrogen bonding facilitated by water leads to the reduced overpotentials for CO_2RR.

Based on the descriptions of the CO_2RR mechanism in the presence of ILs in earlier studies, the role of the IL (in particular the $[EMIM]^+$ cation) and water remains unclear. As ILs behave differently at the interface depending on the choice of the electrode and the electrolyte composition, it has been difficult to develop a unifying understanding regarding the impact of ILs on reaction outcomes at interfaces. We hypothesize that below a critical concentration water acts as a hydrogen bond donor (HBD) as well as a co-catalyst in synergy with $[EMIM]^+$ and does not provide free protons as a proton donor in the reaction. Furthermore, in this study, IL mediated

CO_2RR was revisited with the benchmark [EMIM][BF_4] with a refined focus on the interfacial evolution to clarify the mechanism and the role of $[EMIM]^+$. Specifically, the electric field and the hydrogen bonding effects induced by [EMIM][BF_4] and HBDs, including water and a series of alcohols, in acetonitrile were examined on Ag. By employing voltammetry, in-situ enhanced Raman spectroscopy (SERS), and density functional theory (DFT) calculations, we reveal that the initial electron transfer to CO_2 occurs at reduced overpotentials due to enhanced local electric fields created by reorientation of $[EMIM]^+$ when it is confined between the imidazolium ring plane and the electrode surface. This confinement of CO_2 stabilizes it at the interface and enables its conversion to CO, accompanied by the generation of carbene and water as by-products. Furthermore, our findings suggest water (< 0.5 M) acts as the hydrogen bond donor as opposed to serving as the primary source of free protons. Based on this finding, we further show how the extend of hydrogen bonding as varied by various alcohols alter the microenvironment in synergy with $[EMIM]^+$ at the electrode-electrolyte interface for fine tuning of the thermodynamics of CO_2RR. The clarified role of the imidazolium based ILs and HBDs, and the demonstrated enhancement in CO_2RR will advance non-aqueous electrolyte development and inform future kinetic studies. This study demonstrates that rationally tailored interfacial hydrogen bonding interactions can be used as a design strategy for efficient CO_2 utilization for combined capture and conversion efforts.

RESULTS AND DISCUSSION

[EMIM]$^+$ reorientation induced electric field effects is the reason for lowered overpotential.

Probing the interface with SERS suggests the accumulation and reorientation of [EMIM]$^+$ on Ag with applied negative polarization (**Figure 1a**). Up to -1.5 V vs. Ag/Ag$^+$, the SERS spectra display no notable features other than the acetonitrile -CN stretching mode at 2253 cm^{-1}. As the negative polarization increases, significant spectral changes start to occur, primarily due to the enrichment of the electrode surface with [EMIM]$^+$. In particular, the accumulation of [EMIM]$^+$ starts at -1.5 V vs. Ag/Ag$^+$ (appearance of $\nu_{CH2(N)}$ at 1345 cm^{-1} and $\nu_{CH3(N)}$ at 1376 cm^{-1}) and the orientation changes from tilted to parallel alignment relative to the electrode surface beyond -1.8 V vs. Ag/Ag$^+$ (the red-shift and relative enhancement of the peak at 1345 cm^{-1} compared to the peak at 1376 cm^{-1}), irrespective of the electrolyte saturation with CO_2 or N_2 (Figure S1). Given that [EMIM]$^+$ is typically solvated by an average of four acetonitrile molecules[39, 40] in the bulk electrolyte at the concentration used in this study (0.1 M), the observed behavior suggests that [EMIM]$^+$ starts breaking its solvation shell around -1.5 V vs. Ag/Ag$^+$. As ILs adsorb onto the electrode surface stronger than molecular solvents[41], [EMIM]$^+$ begins to de-solvate, adsorb on the surface and form its own microenvironment. Furthermore, the peak at 1604 cm^{-1} is associated with aromatic C-C stretching and is also present under both CO_2 and N_2. With CO_2 saturation, a new peak at 1610 cm^{-1} emerges at -1.9 V vs. Ag/Ag$^+$. This peak is assigned to the asymmetric stretch of the -COO moiety of the newly formed EMIM-H-COO adduct in accordance with prior reports[42, 43] and in complement of our DFT vibrational calculations of this specie on the Ag surface (1599 cm^{-1}). The asymmetric -COO stretching mode usually overlaps with aromatic ring C-C stretching modes and tends to be weak in the Raman spectrum,[44] as also seen here. Further detailed peak assignments and the associated DFT calculated vibrational frequencies are given in Table S1.

Given the consistent behavior of $[EMIM]^+$ accumulation and orientation at the interface, we examined the local electric field effects induced by these changes using periodic DFT calculations (Quantum ESPRESSO code,[45,46] PBE-D3 functional[47-49]). The calculations were performed using a 4-layer 4×4 Ag(111) slab to model the Ag electrode surface. Additional computational details are provided in the "Density Functional Theory Calculations" section of the SI. The electric field was calculated from the electrostatic potential difference between the combined Ag(111)/$[EMIM]^+$ system relative to the isolated Ag(111) and $[EMIM]^+$ components. The electric field was then calculated from the gradient of this electrostatic potential difference in the orientation of the surface normal. **Figure 1b** shows the calculated electric field in the *xy* plane that intersects the C_2 of $[EMIM]^+$ (highlighted in orange in **Figure 1b**).

The electric field at the C_2 atom is lowest when the $[EMIM]^+$ ring plane is perpendicular to the surface (90°). The general trend shown by these calculations is that the strength and localization of the electric field increase as the angle between the ring plane and the surface decreases. Remarkably, parallel alignment of $[EMIM]^+$ to the electrode surface (0°) enhances the electric field by almost 3-fold compared to vertical alignment (90°). This indicates that the CO_2 in between the imidazolium ring and the electrode experiences a more negative field which further translates to a higher driving force for the first electron transfer reaction. This is what we interpret to be the explanation behind the lowered overpotentials observed. While the electric field effects were previously discussed in literature[15, 50] with the addition of various cations including $[EMIM]^+$, the specific origins of enhancement due to ring orientation in relation to CO_2RR was not explicitly presented through a combined SERS and DFT study.

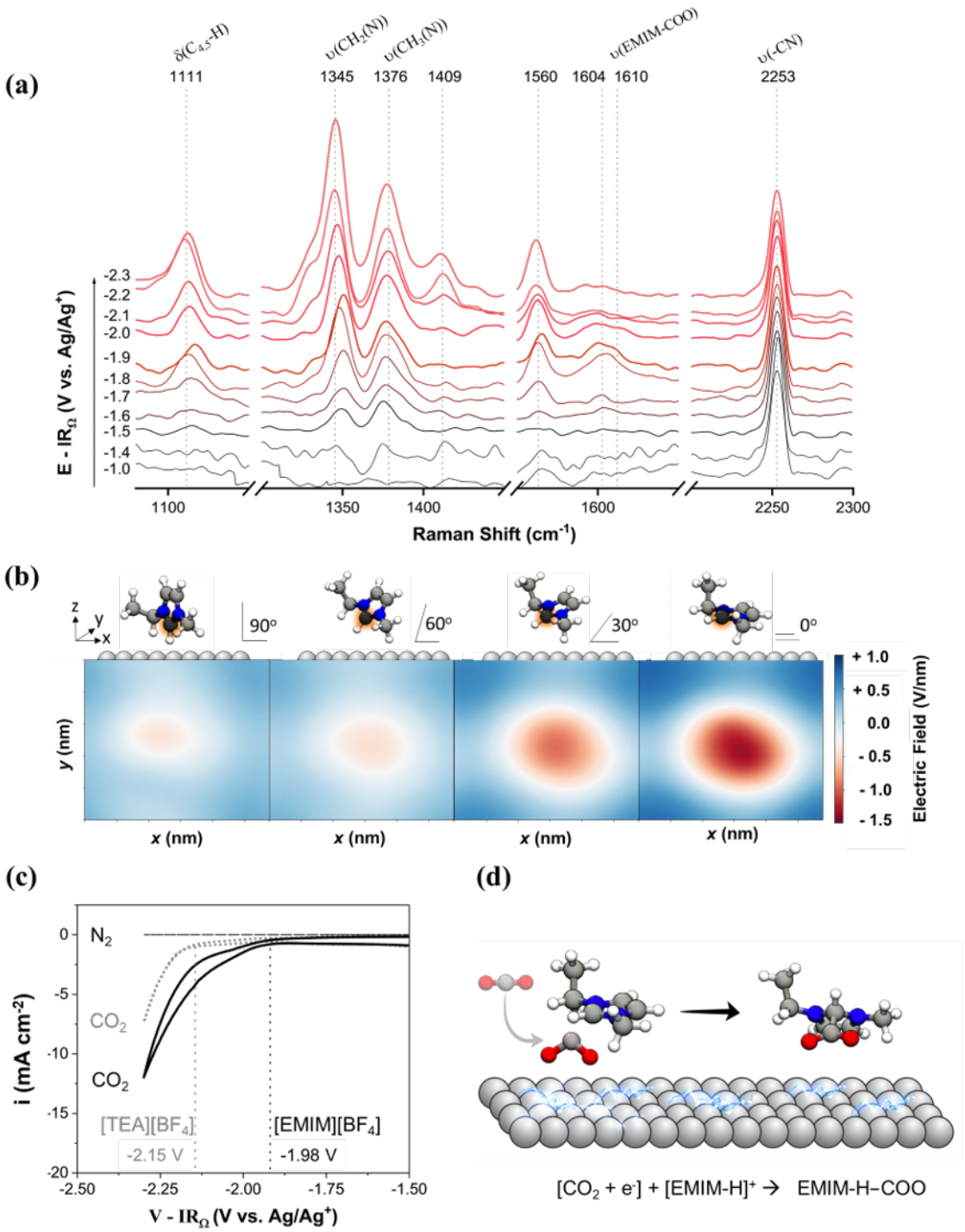

Figure 1. (a) Potential-dependent in-situ SERS spectra for 0.1 M [EMIM][BF_4] in acetonitrile under CO_2 atmosphere. **(b)** Calculated electric field with respect to $[EMIM]^+$ orientation on Ag(111). The electric field is calculated in the *xy* plane intersecting the C_2 atom of $[EMIM]^+$

(highlighted in orange) as the gradient of the electrostatic potential in the *z*-direction normal to the Ag(111) surface. **(c)** CVs of 0.1 M [EMIM][BF_4] (black; solid) under N_2 and CO_2 and 0.1 M [TEA][BF_4] (gray; dotted) under CO_2 on Ag electrode in acetonitrile with 100 mV s^{-1} scan rate. **(d)** Schematics of IL-mediated CO_2RR: the formation of $CO_2^{\bullet-}$ and its interaction with $[EMIM]^+$ to form EMIM-H–COO complex. Atom color code: Ag=gray, C=dark gray, N=blue, H=white, and O=red.

Experimentally, the cyclic voltammetry (CV) curves for the nonaqueous electrolyte of [EMIM][BF_4] in acetonitrile in comparison to the 'control' electrolyte with a quaternary ammonium salt ([TEA][BF_4]), incapable of orientational electric field effects, are shown in **Figure 1c**. Notably, the presence of $[EMIM]^+$ reduces the onset potential of CO_2RR compared to $[TEA]^+$ (from -2.15 to -1.98 V vs. Ag/Ag^+). The absence of faradaic current with 0.1 M IL under N_2 within the potential window where CO_2RR is observed indicates that the first electron transfer is to CO_2, forming the radical anion ($CO_2^{\bullet-}$). Further, the observed onset potential when $[EMIM]^+$ is present closely correlates to that of the potential at which -COO peak of EMIM-H-COO at 1610 cm^{-1} starts to emerge in SERS (-1.9 V vs. Ag/Ag^+ in **Figure 1a**), right after reorientation of $[EMIM]^+$ at -1.8 V vs. Ag/Ag^+.

These observations bring up the question of how CO_2 binds to $[EMIM]^+$ given that CO_2 absorption by bulk imidazolium ILs with [BF_4] anion is typically described as a physisorption process.[51, 52] Because the C_2 atom of $[EMIM]^+$ is highly electrophilic due to its lower electron density and proximity to positively charged nitrogen atoms, it can potentially interact with $CO_2^{\bullet-}$.[53] To further investigate the possible interactions between $[EMIM]^+$ and CO_2 on the electrode surface were analyzed using DFT calculations. We considered different configurations of CO_2 relative to $[EMIM]^+$ on the Ag(111) surface (Figure S2). The calculations show that CO_2 only

binds to the C_2 atom of $[EMIM]^+$ when CO_2 is confined between the $[EMIM]^+$ ring plane and the electrode surface. As shown by the SERS measurements in **Figure 1a**, this parallel configuration of $[EMIM]^+$ to the surface is observed at negative potentials followed with the onset of CO_2 reduction as observed from the appearance of asymmetric stretching peak of -COO moiety at 1610 cm^{-1} and cyclic voltammogram. Therefore, it is concluded that the formation of the adduct between $[EMIM]^+$ and CO_2 is a consequence of the interactions between the cation layer near surface and the newly formed radical anion.

In early days of IL-mediated CO_2RR, it was hypothesized that the mechanistic origin of the experimentally observed decrease in the CO_2RR overpotential involved the formation of CO_2-imidazolium intermediate complexes. However, it has also been reported that this adduct is electrochemically inactive.[29] Furthermore, when the C_2 position is blocked by substituents such as methyl and phenyl, this adduct cannot be formed. Yet, similar early onset potentials (lower overpotentials) with different current responses in CO_2RR were reported even when the C_2 position is blocked by substituents.[38, 54] This reiterates the underlying mechanism of reduced overpotentials for CO_2RR not to be due to the adduct formation as claimed initially in literature. Here, our assertion from the combined SERS, DFT, and CV analysis, is that the catalytic effect is related to enhancement of local electric fields due to voltage-dependent reorientation of $[EMIM]^+$. When CO_2 is situated between the electrode surface and the IL cations it experiences this large electric field, facilitating the initial rate-limiting electron transfer step at more positive potentials than in the absence of IL cations. Because we attribute changes in the CO_2RR onset potential with the interfacial field formed between the electrode and IL cation, we expect CO_2RR catalysis to be influenced by the electrode material and the IL cation. As the ILs are known to form unique double layer structures[13] and specific ion adsorption[55] in some cases, their synergy with the electrode

material determines the potential of zero charge[56] and hence the extent of charge screening to develop the electric field. Different onset potentials for CO_2RR on different electrode materials, as previously shown by Tanner et al.,[57] are expected due to the changes in electric field effects and PZC. Therefore, it is concluded that when CO_2 is confined between $[EMIM]^+$ and the Ag surface, as shown in **Figure 1d**, it is primed to accept its first electron, transitioning into a radical anion at lower overpotentials due to local electric field enhancement as observed in **Figure 1b.**

Utilization of C_2-position during CO_2RR and the effect of water

With clarification of the first electron transfer reaction mechanism, the focus now shifts to unraveling the subsequent stages of the CO_2RR on Ag. As the CO_2RR product on Ag is exclusively CO with the anhydrous electrolyte studied, it becomes imperative to elucidate the fate of CO_2 bound to $[EMIM]^+$ following the first electron transfer at the interface. This transition from the initial electron transfer to the subsequent formation of CO marks distinct intermediary stages in the reaction pathway. DFT calculations were performed to analyze the thermodynamics and kinetics of elementary steps involved in forming key reaction intermediates. We used the computational hydrogen electrode model[58] to calculate potential-dependent reaction free energies for proton-coupled electron transfer steps. We note that such an analysis precludes the calculation of reaction free energies for electron transfer processes that do not involve coupling to a stoichiometric number of protons (further discussion in the SI), such as the initial electron transfer to CO_2 to form the radical anion and the EMIM-H–COO adduct. Therefore, this initial step is not depicted here. Possible intermediates following EMIM-H–COO formation that were examined are shown in **Figure 2**, along with their corresponding free energies. Starting from the formed adduct, the reactions analyzed in **Figure 2** have been proposed in the past; however, most of the literature suggests that the initial electron transfer is to the imidazolium, such as in the study by Wang et

al.[59] Recently, Neyrizi et al.[22] proposed that the initial electron transfer is to CO_2 as we also concluded from the combined in-situ spectro-electrochemistry and computational analysis. Here, the unique perspective is the examination of hydrogen bonding effects on the reaction steps and energetics subsequent to EMIM-H–COO formation.

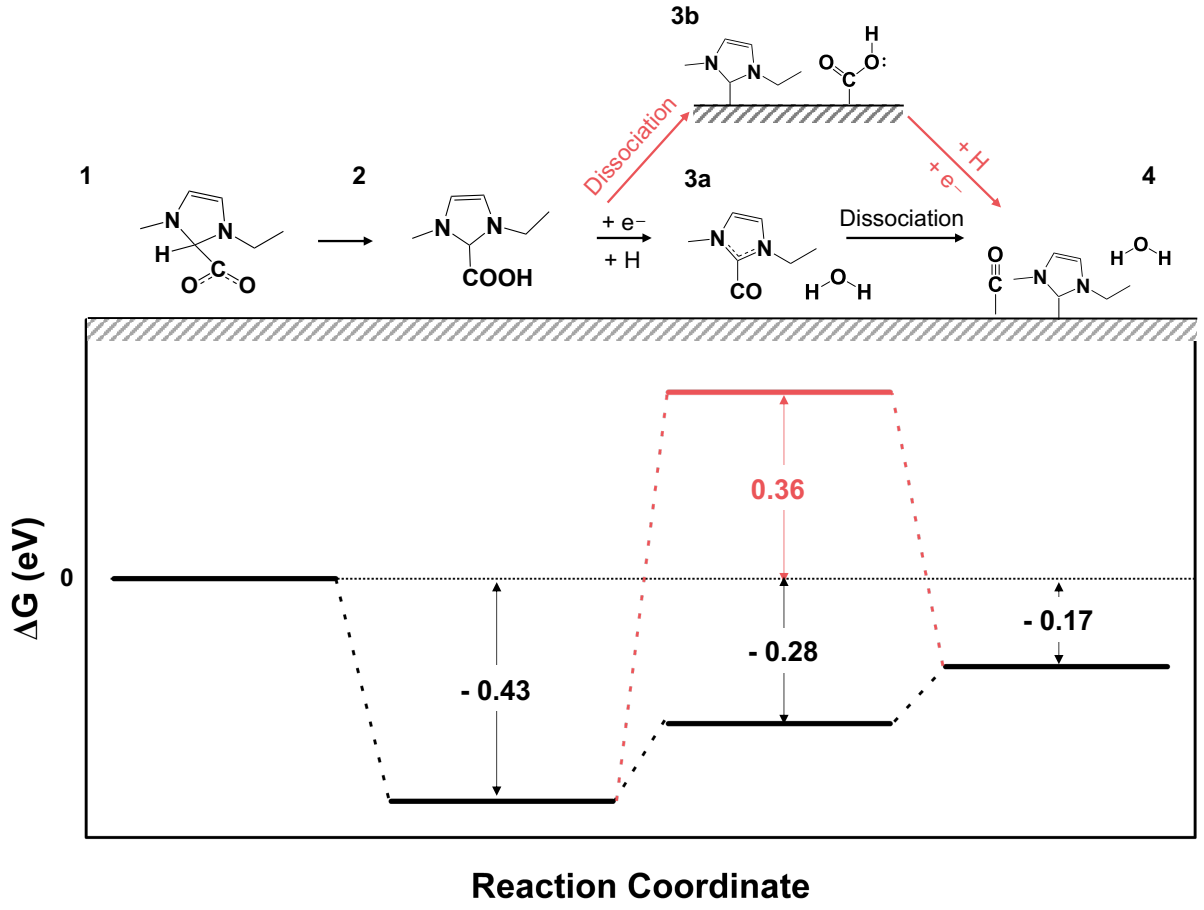

Figure 2. Periodic DFT calculations of the free energy profiles of possible reaction intermediates in $[EMIM]^+$ mediated CO_2 reduction on Ag(111). The calculations suggest a preferred pathway where proton-coupled electron transfer to EMIM-COOH forms EMIM-CO and releases H_2O (intermediate 3a), followed by dissociation to form co-adsorbed EMIM and CO (intermediate 4).

Dissociation of EMIM-COOH on the surface (intermediate 3b) is less thermodynamically favorable.

The DFT calculations shown in **Figure 2** indicate that the more favored route from **1** to **2** (EMIM-COOH) is the hydrogen transfer from C_2-H to the oxygen of -COO^- moiety to form EMIM-COOH. This process is energetically favorable in comparison to the hydrogen transfer from C_2-H to carbon to form EMIM-HCOO (energetic comparison in Figure S4). Charge density difference analysis with DFT shows that oxygen atoms of CO_2 adopt a more negative charge upon EMIM-H–COO adduct formation (Figure S3). Similar analyses were previously used to examine charge redistribution upon redox reactions and bond formation in homogeneous CO_2 catalysis.[60] Electron density accumulates near the oxygen atoms of EMIM-H–COO in this analysis because oxygen is more electronegative than carbon. This charge distribution helps to explain why, in comparison to EMIM-HCOO formation, EMIM-COOH formation is more energetically favorable and exhibits a lower activation barrier.

Proceeding the formation of EMIM-COOH, we considered two possible pathways where the first pathway (black) involves a proton-coupled electron transfer step. This proton-coupled electron transfer step liberates a water molecule and forms EMIM-CO (**3a**). In the subsequent step, the complex dissociates to form co-adsorbed EMIM* carbene and CO* species (**4**). Because CO binds weakly to Ag, [61, 62] it can subsequently desorb as the gaseous product. The adsorbed carbene in **4** can either remain on the surface, thus possibly blocking an active site, or may react with physisorbed CO_2 or water. Conversely, the second pathway (red) posits a dissociation reaction where -COOH moiety detaches from imidazolium ring (**3b**). The hydroxyl group (-OH) lone pair on the adsorbed -COOH proceeds to react with a free proton available to form water and neutral CO (**4**). Since the energetic barriers are higher going from **2** to **3b** than the pathway via **3a**, it is

hypothesized that the reaction follows the first (black) pathway outlined in **Figure 2**, with a rate-limiting step being the first electron transfer to CO_2.

The reaction mechanisms considered in **Figure 2** both require proton transfer from a proton donor, which can impact CO_2RR catalysis and overall CO_2 utilization. The two possible proton donors are either $[EMIM]^+$ or the trace amounts of water in the electrolyte. If $[EMIM]^+$ is the proton donor, the overall reduction reaction with CO_2 to CO will release two carbene species which then can react with other available CO_2 molecules to form carboxylate, [EMIM-COO]. When EMIM-COO carboxylate adducts forms, it is widely accepted that these adducts cannot be further reduced and stay inactive for electrochemical cycle. This results in the reduction of the utilization of available CO_2.[29,63] Therefore, suppressing the formation of EMIM-COO in non-aqueous system is necessary, as discussed later. If H_2O is the proton donor (i.e., $H_2O + e^- \rightarrow *H + OH^-$), the interfacial pH will increase due to generation of OH^- during the reaction. It is well understood that high interfacial pH during CO_2RR in nonaqueous IL electrolytes is associated with (bi)carbonate formation on the electrolyte surface, which has deleterious effects on catalysis.[25]

To investigate the source of protons in the reaction mechanism, experimental measurements were taken to probe water's potential role as a proton donor. We measured Faradaic current related to water reduction to probe whether water is the source of free protons in the reaction. Therefore, the Faradaic current due to hydrogen evolution (0 to 1 M H_2O) under N_2 was examined by differential pulse voltammetry (DPV) (**Figure 3a**), which isolates the Faradaic current from the double-layer charging effects. DPV findings demonstrate minimal water reduction activity for 0.1 M IL in acetonitrile within the same potential range as the CO_2RR when the H_2O concentration is less than 1.0 M. The lack of Faradaic current related to water is further supported by post-electrolysis NMR results (Figure S5), where no spectral changes in $[EMIM]^+$

and water peaks were observed with 0.1 M and 0.3 M H_2O after electrolysis for 2 hours at -2.1 V vs. Ag/Ag^+. However, when the water content increased to 1.0 M, the onset potential for water reduction shifts anodically and the Faradaic current increases. These are results are consistent with the study by Guo et al.[25] which suggests $[EMIM]^+$ to be the proton source for CO formation on Ag in $[EMIM][BF_4]$/acetonitrile electrolyte. They report a consistent Tafel slope between 185 – 179 mV/dec for CO with 0.04 – 0.6 M water content and further increment of water to 1.09 M caused the Tafel slope to drop to 132 mV/dec. They attribute this change in Tafel slope to the contribution of water as a proton source along with $[EMIM]^+$, as evidenced here through DPV. Additional DFT calculations (Figure S6) show that the reaction energies and activation energies for $[EMIM]^+$ dissociation on Ag(111) are significantly lower than for H_2O dissociation, also suggesting that proton transfer from $[EMIM]^+$ is feasible.

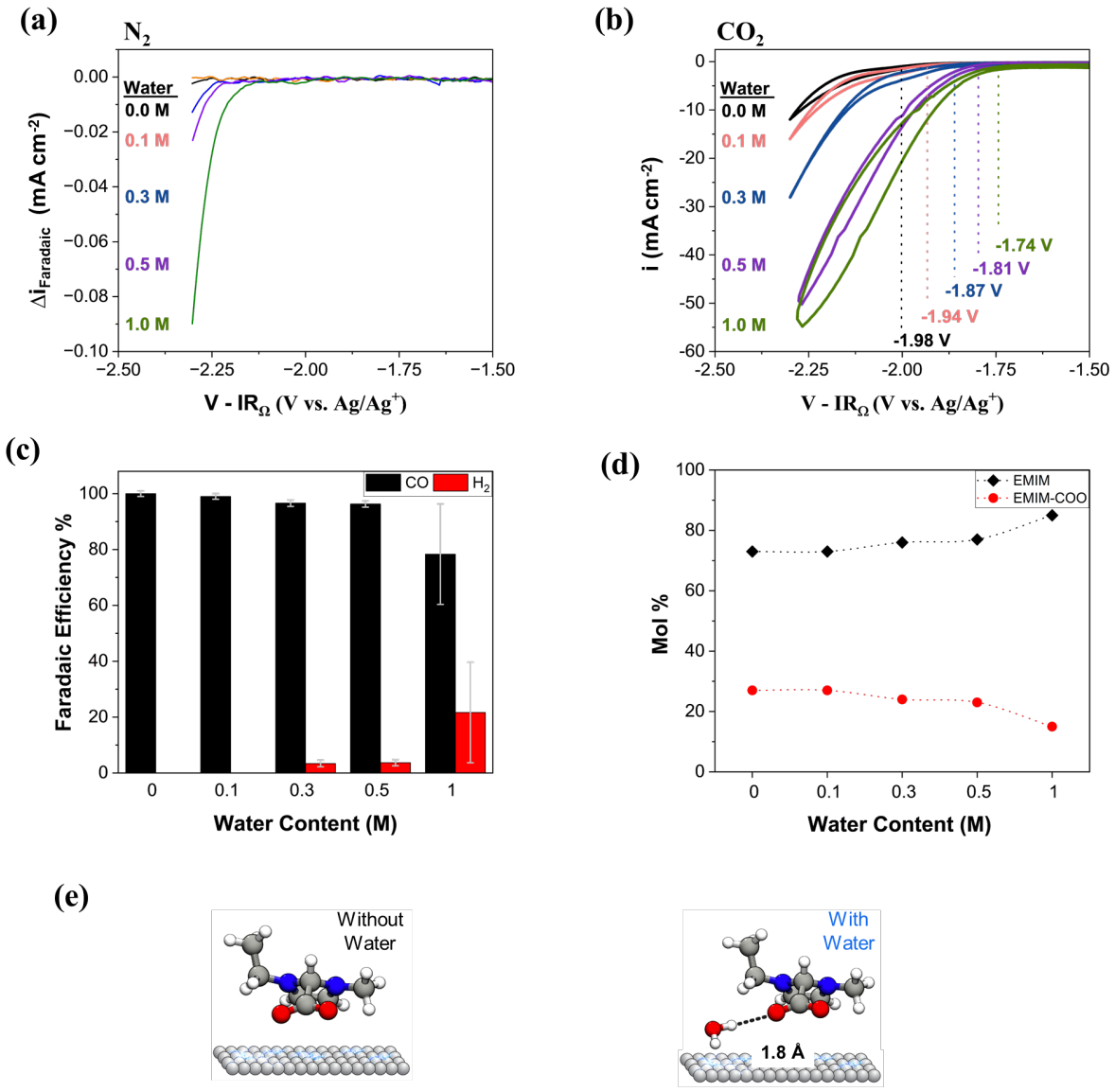

Figure 3. (a) DPV data confirming limited water reduction activity in the CO_2RR potential window, **(b)** CVs showcasing the impact of water on CO_2RR and the resultant shift in onset potential, **(c)** Faradaic efficiencies of electrolytes containing different HBDs after 2 hours of constant potential electrolysis at -2.1 V vs. Ag/Ag^+ on Ag electrode. **(d)** Mole percentages of $[EMIM]^+$ and EMIM-COO after electrolysis as quantified by ^1H NMR. **(e)** Difference in reaction free energies for the EMIM-H–COO formation step with and without water as HBD (blue and

black lines, respectively). The calculated $\Delta\Delta G$ = -0.15 eV indicates that the EMIM-H-COO is stabilized in the presence of water.

Under CO_2, the water addition to the electrolyte shifts the onset potential for CO_2RR from -1.92 V to -1.74 V vs. Ag/Ag^+ as seen in CV curves in **Figure 3b**. Constant potential electrolysis experiments were also performed at -2.1 V vs. Ag/Ag^+ for 2 hours (Figure S7), where a faradaic efficiency greater than 95% for CO was obtained. While H_2 evolution activity up to 0.5 M water concentration remains minimal, consistent with DPV results, increasing water concentration to 1.0 M boosts H_2 evolution faradaic efficiency to 35%. The observed Faradaic activity patterns via DPV and CV, particularly the efficiencies towards CO and H_2 (**Figure 3c**) confirm the hypothesis that water functions primarily as an HBD rather than a source of free protons in the electrolyte up to 0.5 M. Instead, these data suggest that $[EMIM]^+$ is the dominant source of protons and that the overall reaction stoichiometry follows that in eq. (1).

$$3\ CO_2 + 2\ [EMIM]^+ + 2\ e^- \rightarrow CO + 2\ EMIM\text{-}COO + H_2O \quad (1)$$

Furthermore, NMR analysis post electrolysis reveal that 78% of the initial [EMIM] content is preserved without any added water as seen in **Figure 3d**, while the rest is converted to the inactive EMIM-COO adduct (recall eqn. 1). As the water content is increased, a larger fraction of the $[EMIM]^+$ cations are preserved as active components. DFT calculations (Figure S8) suggest a kinetically facile reaction between the carbene and H_2O to regenerate $EMIM^+$, which can proceed with a low 0.2 eV barrier. This reaction can be observed in the broadening of water peak in post-electrolysis NMR results, indicating H_2O to OH conversion (Figure S9). Therefore, although water is not electrochemically reduced, it can chemically react with carbene to regenerate the cation, $[EMIM]^+$. The suppression of inactive EMIM-COO and the regeneration of the $[EMIM]^+$ cation in the presence of water contribute to the enhanced catalytic activity and CO_2 utilization, compared

to the electrolytes without water. Beyond the deprotonation, there is no further degradation of $[EMIM]^+$ that could be detected from NMR (Figure S9) and that the source of CO is from CO_2 as confirmed by GC analysis of electrolysis under N_2 where no CO was detected (Figure S10).

To quantify the role of water as an HBD on electron transfer to CO_2 and EMIM-H-COO adduct formation, we used periodic DFT to calculate the reaction free energies ΔG for adduct formation in the presence and absence of hydrogen bonds to a single H_2O molecule as an HBD. The reaction free energies are defined as:

$$\Delta G_{\mathrm{w/\ H_2O}} = \left[G_{\mathrm{EMIM-H-COO}} - (G_{\mathrm{EMIM}} + \mu_{\mathrm{CO_2}} + \mu_{\mathrm{e}})\right]_{\mathrm{w/\ H_2O}} \quad (2)$$

$$\Delta G_{\mathrm{w/o\ H_2O}} = \left[G_{\mathrm{EMIM-H-COO}} - (G_{\mathrm{EMIM}} + \mu_{\mathrm{CO_2}} + \mu_{\mathrm{e}})\right]_{\mathrm{w/o\ H_2O}} \quad (3)$$

In equations 2 and 3, $G_{\mathrm{EMIM\text{-}H\text{-}COO}}$ is the free energy of adsorbed EMIM-H-COO on the Ag(111) surface, G_{EMIM} is the free energy of the adsorbed $EMIM^+$ cation on the Ag(111) surface, $\mu_{\mathrm{CO_2}}$ is the chemical potential of gas-phase CO_2, and μ_{e} is the chemical potential of an electron. The subscripts "w/ H_2O" and "w/o H_2O" indicate that $G_{\mathrm{EMIM\text{-}H\text{-}COO}}$ and G_{EMIM} are computed in the presence and absence of a single H_2O molecule, respectively. Because we aim to identify the effect of the HBD on the free energy, we calculate a difference between the two ΔG's using the following equation.

$$\Delta\Delta G = \Delta G_{\mathrm{w/\ H_2O}} - \Delta G_{\mathrm{w/o\ H_2O}}$$

$$= [G_{\mathrm{EMIM-H-COO}} - G_{\mathrm{EMIM}}]_{w\ H2O} - [G_{\mathrm{EMIM-H-COO}} - G_{\mathrm{EMIM}}]_{\mathrm{w/o\ H_2O}} \quad (4)$$

Note that in this analysis, the CO_2 and electron reference states cancel. This analysis is depicted in **Figure 3e**, which the calculated $\Delta\Delta G$ calculated for the first electron transfer to CO_2 followed by the spontaneous nucleophilic interaction with the $[EMIM]^+$ layer in the absence and presence of hydrogen bonds with a single H_2O molecule. Our DFT calculations give a $\Delta\Delta G$ of -0.15 eV, which indicates that the EMIM-H-COO is stabilized when hydrogen bonding with a single H_2O molecule.

This result shows that HBDs such as water can decrease the ΔG for the first step of CO_2RR, which is expected to reduce overall overpotentials.

We note that the computational model shown in **Figure 3e** is a simplified model of the interfacial reaction because it does not include a full description of [EMIM][BF_4] /acetonitrile electrolyte at the interface. A fully atomistic model of the non-aqueous IL electrolyte would be highly sensitive to initial configurations and is not trivial to capture with sufficient accuracy using standard continuum solvation models. An extensive analysis of the solvation effects would require sampling with molecular dynamics. While the exclusion of solvation effects is expected to affect absolute values of calculated reaction free energies, we note that the DFT calculations herein are focused on modeling chemical reactions involving the desolvated $[EMIM]^+$ at the electrode surface. Thus, we expect these calculations to provide reliable trends between the systems with and without HBDs. The trend in **Figure 3e** is instead meant to provide a qualitative description of the effects that HBDs such as water may play during catalysis, rather than a quantitative prediction of changes in overpotential with HBDs. It is important to highlight that the role of water as an HBD extends to later stages in the reaction scheme, including the formation of EMIM-COOH from the EMIM-H-COO adduct (Figure S11). The decrease in energetics necessary for EMIM-COOH formation step aligns with the findings of Braunschweig et al. [35] where the onset potential for EMIM-COOH formation closely correlated with the water content, without water being consumed in the process. Furthermore, DFT calculations in Figure S11 also show the effect of HBD on CO_2RR energetics for the high energy pathway following EMIM-COOH formation (i.e., pathway 3b shown in **Figure 2**). Across the four reaction steps examined, the ΔG and activation energy for each step decreases when water is present as HBD.

The considerable decrease in energy requirements, alongside the overall stabilization of intermediate stages, emphasizes the crucial role played by hydrogen bonding networks. This observation holds particular significance given the diverse compositions and water concentrations utilized in electrolytes across the literature, leading to varied mechanistic interpretations. The results depicted in **Figure 3** underscore the importance of electrolyte composition in modulating catalytic activity.

Modulating hydrogen bonding network controls the onset potential of CO_2RR

As the ability of an electrolyte to engage in hydrogen bonding can profoundly influence CO_2RR, a systematic set of HBDs were examined to understand the mechanistic role of the HBD as a function of its hydrogen bonding strength. The HBDs presented in **Figure 4a** represent structural variations inspired from water, encompassing variations in alkyl chain length and the number of -OH functional groups. Among the single-functional donors, the addition of 0.1 M ethanol to the 0.1 M IL in acetonitrile demonstrates a greater shift in onset potential compared to 0.1 M methanol (ΔE_{onset} is 80 mV for ethanol and 50 mV for methanol), as illustrated in the CVs presented in **Figure 4b**. Notably, these shifts surpass those observed with the addition of 0.1 M water (ΔE_{onset} = 40 mV). Similarly, 0.1 M ethylene glycol (EG) induces a greater shift than its longer counterpart, 0.1 M propylene glycol (PG) (140 and 110 mV for EG and PG, respectively). Lastly, glycerol (Gly) with its three -OH functional groups, demonstrates the greatest positive shift in onset potential, by 160 mV. The enhancement in onset potential is attributed to the higher number of -OH functionalities in the HBD structure.

The polar characteristics of an electrolyte can indicate its ability to donate or accept hydrogen bonds and generate dipole moments under the influence of an external electric field, thereby resulting in dipole-dipole interactions. To discern the primary interactions responsible for

shifting the onset potential of CO_2 reduction, Kamlet-Taft parameters were calculated (Table S2) using two distinct dyes (Betaine Dye 30 and DENA) with UV-Vis spectroscopy (Figure S12). These parameters offer insights into the bulk properties of electrolytes, including the polarizability (π^*) – *a measure of dipole interactions*, and the hydrogen bond acidity (α) – *a measure of hydrogen bonding ability* (**Figure 4c**). This analysis demonstrates that while polarizability (black curve) remains consistent with the addition of HBDs into 0.1 M IL in acetonitrile, the propensity for hydrogen bond formation (red curve) gradually increases upon the introduction of water, ethylene glycol and glycerol.

To further investigate the effect of hydrogen bonding network at the electrode-electrolyte interface, 1 mM anthraquinone (AQ) was employed under N_2 atmosphere as UV-Vis spectroscopy revealed no detectable change in bulk electrolyte characteristics upon CO_2 saturation (Figure S12). Quinones undergo a two-step reduction ($Q \rightarrow Q^{\bullet -} \rightarrow Q^{-2}$), with the second reduction step being sensitive to the hydrogen bonding network in the electrolyte[64, 65] (Figure S13).

Insights into the hydrogen bonding network at the interface can be gleaned by probing the interface with AQ, which also produces radical anions during the reduction process, and parallels to the CO_2RR can be drawn. **Figure 4d** illustrates the shift in the second reduction peak of AQ upon the addition of different HBDs to 0.1 M IL in acetonitrile. As the water content increases, the second reduction peak undergoes a progressive shift from -1.62 V vs. Ag/Ag^+ for the solution containing only 0.1 M IL in acetonitrile to -1.30 V vs. Ag/Ag^+ with the addition of 1.0 M water. Notably, the introduction of 0.1 M EG to the electrolyte causes the second reduction peak of AQ to shift to -1.38 V vs. Ag/Ag^+, while the addition of 0.1 M Gly further shifts the peak to -1.29 V vs. Ag/Ag^+.

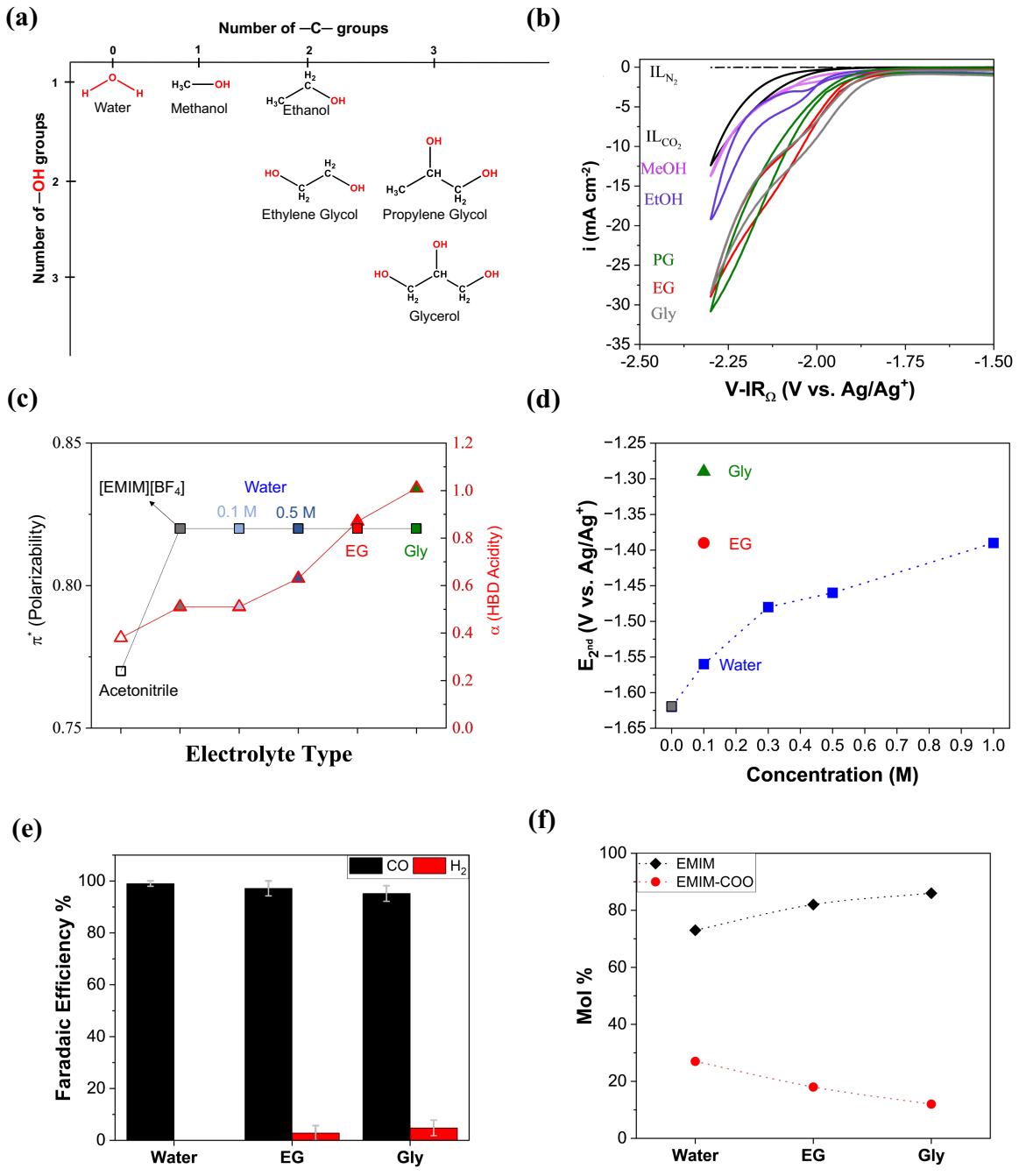

Figure 4. (a) Structures of HBDs examined; **(b)** CVs of electrolytes with 0.1 M HBD additions to IL/acetonitrile on Ag with 100 mV s^{-1} scan rate ; **(c)** Kamlet-Taft parameters calculated via UV-Vis spectroscopy, **(d)** The change in second reduction peak of anthraquinone upon additions HBDs, **(e)** Faradaic efficiencies of electrolytes containing different HBDs after 2 hours of constant

potential electrolysis at -2.1 V vs. Ag/Ag^+ on Ag electrode. **(f)** Mol percentages of $[EMIM]^+$ and carboxylate after electrolysis.

The investigation into the local hydrogen bonding network at the interface using transient voltammetry with AQ, along with the analysis of the properties of electrolytes using UV-Vis spectroscopy, provides compelling evidence for the enhanced hydrogen bonding capability of the microenvironment for CO_2RR. As a result, the observed shift in the onset potential of CO_2RR can be attributed to the strengthening of the hydrogen bonding network facilitated by the addition of HBDs, which remain electrochemically stable within the operational electrochemical window of CO_2RR (Figure S14). It should be noted that the presence of water previously reported to facilitate the structural changes of Im-based cations at earlier potentials at the interface by lubricating the IL layers. [66] Even though the shift observed is attributed to the strengthening of hydrogen bonding network in the light of above-mentioned investigations, the influence of alcohols on the re-orientation of Im-ring and the local solvation environment on the electrode surface warrants further investigation to understand the interplay between hydrogen bonding interactions and the orientational behavior of the cation at the electrode surface.

Finally, constant potential electrolysis experiments conducted at -2.1 V vs. Ag/Ag^+ reaffirm a faradaic efficiency exceeding 95% for CO as seen in **Figure 4e** (see chronoamperometry curves in Figure S15). Intriguingly, the presence of 0.1 M EG and Gly leads to a more effective suppression of EMIM-COO formation (82 % and 86%, respectively) compared to 0.1 M water (73 %), as depicted in **Figure 4f**. Post-electrolysis NMR analysis (Figure S16) indicates no alteration in the HBD structures. Taken together, the cyclic voltammetry (Figure S14) and post-electrolysis NMR data (Figure S16) indicate that EG and Gly are stable against decomposition within the potential window of CO_2 reduction. Thus, the H_2 activity shown in **Figure 4e** (mostly observed

towards the end of electrolysis period within 2 hours) is attributed to residual and in-situ produced water reduction.

CONCLUSION

This study demonstrates the electric field and hydrogen bonding effects in IL-mediated CO_2RR. Voltage-dependent orientation of $[EMIM]^+$ is shown to induce electric field effects where the CO_2 confined between the imidazolium ring and the electrode surface gets stabilized to receive the first electron transfer in CO_2RR. Proceeding this step involves proton mobilization from $[EMIM]^+$ as demonstrated by transient voltammetry and DFT calculations. The following steps involve the formation of EMIM-COOH that ultimately yields CO and carbene. The carbene specie can further form EMIM-COO, thus reducing CO_2 utilization. Water, often considered as a proton source, was found to function as an HBD instead, up to a critical concentration. Furthermore, CO_2RR steps are shown to be sensitive to the hydrogen bonding network at the interface. The augmentation of the hydrogen bonding network through the addition of alcohols as HBDs suppresses the inactive EMIM-COO formation more effectively compared to water and increases the catalytic activity. This new understanding on the role of HBDs provides a new aspect to tune electrocatalytic reactions in non-aqueous electrolytes, especially in the case of capture and conversion of CO_2.

ASSOCIATED CONTENT

Supporting Information

The Supporting Information is available at XXX. Detailed experimental and computational methods; SERS spectra under N_2 and detailed peak assignments, Chronoamperometry curves, NMR spectra and analysis, and free energy change diagrams for reactions.

Notes

The authors declare no competing financial interest.

Acknowledgements

This study was primarily funded by B.G.'s NSF CAREER award (no. 2045111) from the Division of Chemical, Bioengineering, Environmental and Transport Systems (CBET), Interfacial Engineering, and Electrochemical Systems. Partial support for O.K.C. for probing the interface with quinone informer was from an NSF award (no.1904592) from Division of Chemistry. Z.B., V.K., and R.E.W. were supported by Breakthrough Electrolytes for Energy Storage (BEES2) – an Energy Frontier Research Center (EFRC) of the U.S. Department of Energy, Office of Science, Basic Energy Sciences under Award No. DE-SC0019409 for DFT calculations and polarity measurements. S.D. was supported by the Center for Closing the Carbon Cycle (4C) EFRC, under award # DE-SC0023427, for electrolysis product analysis. This work made use of the High Performance Computing Resource in the Core Facility for Advanced Research Computing at Case Western Reserve University and the Ohio Supercomputer Center, Columbus, OH.[67] This research used resources of the National Energy Research Scientific Computing Center, a DOE Office of Science User Facility supported by the Office of Science of the U.S. Department of Energy under Contract No. DE-AC02-05CH11231 using NERSC award BES-ERCAP0027121. The authors would like to thank the UV-Vis and Raman Spectroscopy at the Department of Chemical Engineering in addition to the NMR Instrumentation Facility at the Department of Chemistry at Case Western Reserve University for access to instrumentation.

References

(1) Bard, A. J. Inner-Sphere Heterogeneous Electrode Reactions. Electrocatalysis and Photocatalysis: The Challenge. *Journal of the American Chemical Society* **2010**, *132* (22), 7559-7567. DOI: 10.1021/ja101578m.

(2) Dunwell, M.; Yan, Y.; Xu, B. Understanding the influence of the electrochemical double-layer on heterogeneous electrochemical reactions. *Current Opinion in Chemical Engineering* **2018**, *20*, 151-158. DOI: https://doi.org/10.1016/j.coche.2018.05.003.

(3) Tan, Z.; Zhang, J.; Yang, Y.; Zhong, J.; Zhao, Y.; Hu, J.; Han, B.; Chen, Z. Alkaline Ionic Liquid Microphase Promotes Deep Reduction of CO_2 on Copper. *Journal of the American Chemical Society* **2023**, *145* (40), 21983-21990. DOI: 10.1021/jacs.3c06860.

(4) Lee, S. Y.; Kim, J.; Bak, G.; Lee, E.; Kim, D.; Yoo, S.; Kim, J.; Yun, H.; Hwang, Y. J. Probing Cation Effects on *CO Intermediates from Electroreduction of CO_2 through Operando Raman Spectroscopy. *Journal of the American Chemical Society* **2023**, *145* (42), 23068-23075. DOI: 10.1021/jacs.3c05799.

(5) Paik, W.; Andersen, T. N.; Eyring, H. Kinetic studies of the electrolytic reduction of carbon dioxide on the mercury electrode. *Electrochimica Acta* **1969**, *14* (12), 1217-1232. DOI: https://doi.org/10.1016/0013-4686(69)87019-2.

(6) Amatore, C.; Saveant, J. M. Mechanism and kinetic characteristics of the electrochemical reduction of carbon dioxide in media of low proton availability. *Journal of the American Chemical Society* **1981**, *103* (17), 5021-5023. DOI: 10.1021/ja00407a008.

(7) Rosen, B. A.; Salehi-Khojin, A.; Thorson, M. R.; Zhu, W.; Whipple, D. T.; Kenis, P. J. A.; Masel, R. I. Ionic Liquid–Mediated Selective Conversion of CO_2 to CO at Low Overpotentials. *Science* **2011**, *334* (6056), 643-644. DOI: 10.1126/science.1209786.

(8) Urushihara, M.; Chan, K.; Shi, C.; Nørskov, J. K. Theoretical study of $EMIM^+$ adsorption on silver electrode surfaces. *The Journal of Physical Chemistry C* **2015**, *119* (34), 20023-20029.

(9) Imai, M.; Tanabe, I.; Sato, T.; Fukui, K.-i. Local structures and dynamics of interfacial imidazolium-based ionic liquid depending on the electrode potential using electrochemical attenuated total reflectance ultraviolet spectroscopy. *Spectrochimica Acta Part A: Molecular and Biomolecular Spectroscopy* **2022**, *273*, 121040. DOI: https://doi.org/10.1016/j.saa.2022.121040.

(10) Coskun, O. K.; Dongare, S.; Doherty, B.; Klemm, A.; Tuckerman, M.; Gurkan, B. Tailoring Electrochemical CO_2 Reduction on Copper by Reactive Ionic Liquid and Native Hydrogen Bond Donors. *Angewandte Chemie* **2024**, *136* (1), e202312163.

(11) Santos, V. O.; Alves, M. B.; Carvalho, M. S.; Suarez, P. A. Z.; Rubim, J. C. Surface-Enhanced Raman Scattering at the Silver Electrode/Ionic Liquid (BMIPF6) Interface. *The Journal of Physical Chemistry B* **2006**, *110* (41), 20379-20385. DOI: 10.1021/jp0643348.

(12) Yuan, Y.-X.; Niu, T.-C.; Xu, M.-M.; Yao, J.-L.; Gu, R.-A. Probing the adsorption of methylimidazole at ionic liquids/Cu electrode interface by surface-enhanced Raman scattering spectroscopy. *Journal of Raman Spectroscopy* **2010**, *41* (5), 516-523. DOI: https://doi.org/10.1002/jrs.2480.

(13) Coskun, O. K.; Muñoz, M.; Dongare, S.; Dean, W.; Gurkan, B. E. Understanding the Electrode–Electrolyte Interfaces of Ionic Liquids and Deep Eutectic Solvents. *Langmuir* **2024**, *40* (7), 3283-3300. DOI: 10.1021/acs.langmuir.3c03397.

(14) García Rey, N.; Dlott, D. D. Structural Transition in an Ionic Liquid Controls CO_2 Electrochemical Reduction. *The Journal of Physical Chemistry C* **2015**, *119* (36), 20892-20899. DOI: 10.1021/acs.jpcc.5b03397.

(15) Chen, L. D.; Urushihara, M.; Chan, K.; Nørskov, J. K. Electric Field Effects in Electrochemical CO_2 Reduction. *ACS Catalysis* **2016**, *6* (10), 7133-7139. DOI: 10.1021/acscatal.6b02299.

(16) Liu, B.; Guo, W.; Gebbie, M. A. Tuning Ionic Screening To Accelerate Electrochemical CO_2 Reduction in Ionic Liquid Electrolytes. *ACS Catalysis* **2022**, *12* (15), 9706-9716. DOI: 10.1021/acscatal.2c02154.

(17) Kemna, A.; García Rey, N.; Braunschweig, B. Mechanistic Insights on CO_2 Reduction Reactions at Platinum/[BMIM][BF4] Interfaces from In Operando Spectroscopy. *ACS Catalysis* **2019**, *9* (7), 6284-6292. DOI: 10.1021/acscatal.9b01033.

(18) Michez, R.; Doneux, T.; Buess-Herman, C.; Luhmer, M. NMR study of the reductive decomposition of [bmim][NTf2] at gold electrodes and indirect electrochemical conversion of CO_2. *ChemPhysChem* **2017**, *18* (16), 2208-2216.

(19) Wang, Y.; Hayashi, T.; He, D.; Li, Y.; Jin, F.; Nakamura, R. A reduced imidazolium cation layer serves as the active site for electrochemical carbon dioxide reduction. *Applied Catalysis B: Environmental* **2020**, *264*, 118495. DOI: https://doi.org/10.1016/j.apcatb.2019.118495.

(20) Wang, Y.; Hatakeyama, M.; Ogata, K.; Wakabayashi, M.; Jin, F.; Nakamura, S. Activation of CO_2 by ionic liquid EMIM–BF_4 in the electrochemical system: A theoretical study. *Physical Chemistry Chemical Physics* **2015**, *17* (36), 23521-23531.

(21) Hanc-Scherer, F. A.; Montiel, M. A.; Montiel, V.; Herrero, E.; Sánchez-Sánchez, C. M. Surface structured platinum electrodes for the electrochemical reduction of carbon dioxide in imidazolium based ionic liquids. *Physical Chemistry Chemical Physics* **2015**, *17* (37), 23909-23916, DOI: 10.1039/C5CP02361K.

(22) Neyrizi, S.; Kiewiet, J.; Hempenius, M. A.; Mul, G. What It Takes for Imidazolium Cations to Promote Electrochemical Reduction of CO_2. *ACS Energy Letters* **2022**, *7* (10), 3439-3446. DOI: 10.1021/acsenergylett.2c01372.

(23) Motobayashi, K.; Maeno, Y.; Ikeda, K. In Situ Spectroscopic Characterization of an Intermediate of CO_2 Electroreduction on a Au Electrode in Room-Temperature Ionic Liquids. *The Journal of Physical Chemistry C* **2022**, *126* (29), 11981-11986. DOI: 10.1021/acs.jpcc.2c03012.

(24) Papasizza, M.; Cuesta, A. In Situ Monitoring Using ATR-SEIRAS of the Electrocatalytic Reduction of CO_2 on Au in an Ionic Liquid/Water Mixture. *ACS Catalysis* **2018**, *8* (7), 6345-6352. DOI: 10.1021/acscatal.8b00977.

(25) Guo, W.; Liu, B.; Gebbie, M. A. Suppressing Co-Ion Generation via Cationic Proton Donors to Amplify Driving Forces for Electrochemical CO_2 Reduction. *The Journal of Physical Chemistry C* **2023**, *127* (29), 14243-14254. DOI: 10.1021/acs.jpcc.3c04004.

(26) Dongare, S.; Coskun, O. K.; Cagli, E.; Lee, K. Y. C.; Rao, G.; Britt, R. D.; Berben, L. A.; Gurkan, B. A Bifunctional Ionic Liquid for Capture and Electrochemical Conversion of CO_2 to CO over Silver. *ACS Catalysis* **2023**, *13* (12), 7812-7821. DOI: 10.1021/acscatal.3c01538.

(27) Marjolin, A.; Keith, J. A. Thermodynamic Descriptors for Molecules That Catalyze Efficient CO_2 Electroreductions. *ACS Catalysis* **2015**, *5* (2), 1123-1130. DOI: 10.1021/cs501406j.

(28) Fortunati, A.; Risplendi, F.; Re Fiorentin, M.; Cicero, G.; Parisi, E.; Castellino, M.; Simone, E.; Iliev, B.; Schubert, T. J. S.; Russo, N.; et al. Understanding the role of imidazolium-based ionic liquids in the electrochemical CO_2 reduction reaction. *Communications Chemistry* **2023**, *6* (1), 84. DOI: 10.1038/s42004-023-00875-9.

(29) Sun, L.; Ramesha, G. K.; Kamat, P. V.; Brennecke, J. F. Switching the Reaction Course of Electrochemical CO_2 Reduction with Ionic Liquids. *Langmuir* **2014**, *30* (21), 6302-6308. DOI: 10.1021/la5009076.

(30) Feroci, M.; Chiarotto, I.; Ciprioti, S. V.; Inesi, A. On the reactivity and stability of electrogenerated N-heterocyclic carbene in parent 1-butyl-3-methyl-1H-imidazolium tetrafluoroborate: Formation and use of N-heterocyclic carbene-CO_2 adduct as latent catalyst. *Electrochimica Acta* **2013**, *109*, 95-101. DOI: https://doi.org/10.1016/j.electacta.2013.07.115.

(31) Van Ausdall, B. R.; Glass, J. L.; Wiggins, K. M.; Aarif, A. M.; Louie, J. A Systematic Investigation of Factors Influencing the Decarboxylation of Imidazolium Carboxylates. *The Journal of Organic Chemistry* **2009**, *74* (20), 7935-7942. DOI: 10.1021/jo901791k.

(32) Zhao, S.-F.; Horne, M.; Bond, A. M.; Zhang, J. Is the Imidazolium Cation a Unique Promoter for Electrocatalytic Reduction of Carbon Dioxide? *The Journal of Physical Chemistry C* **2016**, *120* (42), 23989-24001. DOI: 10.1021/acs.jpcc.6b08182.

(33) Moura de Salles Pupo, M.; Kortlever, R. Electrolyte Effects on the Electrochemical Reduction of CO_2. *ChemPhysChem* **2019**, *20* (22), 2926-2935. DOI: https://doi.org/10.1002/cphc.201900680

(34) Sharifi Golru, S.; Biddinger, E. J. Effect of additives in aqueous electrolytes on CO_2 electroreduction. *Chemical Engineering Journal* **2022**, *428*, 131303. DOI: https://doi.org/10.1016/j.cej.2021.131303.

(35) Ratschmeier, B.; Kemna, A.; Braunschweig, B. Role of H_2O for CO_2 Reduction Reactions at Platinum/Electrolyte Interfaces in Imidazolium Room-Temperature Ionic Liquids. *ChemElectroChem* **2020**, *7* (7), 1765-1774. DOI: 10.1002/celc.202000316.

(36) Lim, H.-K.; Kwon, Y.; Kim, H. S.; Jeon, J.; Kim, Y.-H.; Lim, J.-A.; Kim, B.-S.; Choi, J.; Kim, H. Insight into the Microenvironments of the Metal–Ionic Liquid Interface during Electrochemical CO_2 Reduction. *ACS Catalysis* **2018**, *8* (3), 2420-2427. DOI: 10.1021/acscatal.7b03777.

(37) Yang, X.-H.; Papasizza, M.; Cuesta, A.; Cheng, J. Water-In-Salt Environment Reduces the Overpotential for Reduction of CO_2 to CO_2^- in Ionic Liquid/Water Mixtures. *ACS Catalysis* **2022**, *12* (11), 6770-6780. DOI: 10.1021/acscatal.2c00395.

(38) Lau, G. P. S.; Schreier, M.; Vasilyev, D.; Scopelliti, R.; Grätzel, M.; Dyson, P. J. New Insights Into the Role of Imidazolium-Based Promoters for the Electroreduction of CO_2 on a Silver

Electrode. *Journal of the American Chemical Society* **2016**, *138* (25), 7820-7823. DOI: 10.1021/jacs.6b03366.

(39) Bešter-Rogač, M.; Stoppa, A.; Buchner, R. Ion Association of Imidazolium Ionic Liquids in Acetonitrile. *The Journal of Physical Chemistry B* **2014**, *118* (5), 1426-1435. DOI: 10.1021/jp412344a.

(40) Stoppa, A.; Hunger, J.; Hefter, G.; Buchner, R. Structure and Dynamics of 1-N-Alkyl-3-N-Methylimidazolium Tetrafluoroborate + Acetonitrile Mixtures. *The Journal of Physical Chemistry B* **2012**, *116* (25), 7509-7521. DOI: 10.1021/jp3020673.

(41) Endres, F.; Höfft, O.; Borisenko, N.; Gasparotto, L. H.; Prowald, A.; Al-Salman, R.; Carstens, T.; Atkin, R.; Bund, A.; Zein El Abedin, S. Do solvation layers of ionic liquids influence electrochemical reactions? *Physical Chemistry Chemical Physics* **2010**, *12* (8), 1724-1732, DOI: 10.1039/B923527M.

(42) Socrates, G. *Infrared and Raman characteristic group frequencies: tables and charts*; John Wiley & Sons, 2004.

(43) Jiang, S.; Klingan, K.; Pasquini, C.; Dau, H. New aspects of operando Raman spectroscopy applied to electrochemical CO_2 reduction on Cu foams. *The Journal of Chemical Physics* **2018**, *150* (4). DOI: 10.1063/1.5054109.

(44) Firkala, T.; Tálas, E.; Kristyán, S.; Szöllősi, G.; Drotár, E.; Mink, J.; Mihály, J. Surface enhanced Raman spectroscopic (SERS) behavior of substituted propenoic acids used in heterogeneous catalytic asymmetric hydrogenation. *Journal of Raman Spectroscopy* **2015**, *46* (11), 1102-1109. DOI: https://doi.org/10.1002/jrs.4741.

(45) Giannozzi, P.; Baroni, S.; Bonini, N.; Calandra, M.; Car, R.; Cavazzoni, C.; Ceresoli, D.; Chiarotti, G. L.; Cococcioni, M.; Dabo, I. QUANTUM ESPRESSO: a modular and open-source software project for quantum simulations of materials. *Journal of physics: Condensed matter* **2009**, *21* (39), 395502.

(46) Giannozzi, P.; Andreussi, O.; Brumme, T.; Bunau, O.; Buongiorno Nardelli, M.; Calandra, M.; Car, R.; Cavazzoni, C.; Ceresoli, D.; Cococcioni, M.; et al. Advanced capabilities for materials modelling with Quantum ESPRESSO. *Journal of Physics: Condensed Matter* **2017**, *29* (46), 465901. DOI: 10.1088/1361-648X/aa8f79.

(47) Perdew, J. P.; Burke, K.; Wang, Y. Generalized gradient approximation for the exchange-correlation hole of a many-electron system. *Physical Review B* **1996**, *54* (23), 16533-16539. DOI: 10.1103/PhysRevB.54.16533.

(48) Grimme, S.; Antony, J.; Ehrlich, S.; Krieg, H. A consistent and accurate ab initio parametrization of density functional dispersion correction (DFT-D) for the 94 elements H-Pu. *The Journal of Chemical Physics* **2010**, *132* (15). DOI: 10.1063/1.3382344.

(49) Grimme, S.; Ehrlich, S.; Goerigk, L. Effect of the damping function in dispersion corrected density functional theory. *Journal of Computational Chemistry* **2011**, *32* (7), 1456-1465. DOI: https://doi.org/10.1002/jcc.21759.

(50) García Rey, N.; Dlott, D. D. Structural transition in an ionic liquid controls CO2 electrochemical reduction. *The Journal of Physical Chemistry C* **2015**, *119* (36), 20892-20899.

(51) Shiflett, M. B.; Yokozeki, A. Solubilities and Diffusivities of Carbon Dioxide in Ionic Liquids: [bmim][PF_6] and [bmim][BF_4]. *Industrial & Engineering Chemistry Research* **2005**, *44* (12), 4453-4464. DOI: 10.1021/ie058003d.

(52) Lei, Z.; Yuan, J.; Zhu, J. Solubility of CO_2 in Propanone, 1-Ethyl-3-methylimidazolium Tetrafluoroborate, and Their Mixtures. *Journal of Chemical & Engineering Data* **2010**, *55* (10), 4190-4194. DOI: 10.1021/je100343v.

(53) Ennis, E.; Handy, T. S. The Chemistry of the C2 Position of Imidazolium Room Temperature Ionic Liquids. *Current Organic Synthesis* **2007**, *4* (4), 381-389. DOI: http://dx.doi.org/10.2174/157017907782408824.

(54) Noh, S.; Cho, Y. J.; Zhang, G.; Schreier, M. Insight into the Role of Entropy in Promoting Electrochemical CO_2 Reduction by Imidazolium Cations. *Journal of the American Chemical Society* **2023**, *145* (50), 27657-27663. DOI: 10.1021/jacs.3c09687.

(55) Rudnev, A. V.; Kiran, K.; Broekmann, P. Specific cation adsorption: Exploring synergistic effects on CO_2 electroreduction in ionic liquids. *ChemElectroChem* **2020**, *7* (8), 1897-1903.

(56) Costa, R.; Pereira, C. M.; Silva, A. F. Charge storage on ionic liquid electric double layer: the role of the electrode material. *Electrochimica Acta* **2015**, *167*, 421-428.

(57) Tanner, E. E.; Batchelor-McAuley, C.; Compton, R. G. Carbon dioxide reduction in room-temperature ionic liquids: the effect of the choice of electrode material, cation, and anion. *The Journal of Physical Chemistry C* **2016**, *120* (46), 26442-26447.

(58) Nørskov, J. K.; Rossmeisl, J.; Logadottir, A.; Lindqvist, L.; Kitchin, J. R.; Bligaard, T.; Jonsson, H. Origin of the overpotential for oxygen reduction at a fuel-cell cathode. *The Journal of Physical Chemistry B* **2004**, *108* (46), 17886-17892.

(59) Wang, Y.; Hatakeyama, M.; Ogata, K.; Wakabayashi, M.; Jin, F.; Nakamura, S. Activation of CO_2 by ionic liquid EMIM–BF_4 in the electrochemical system: a theoretical study. *Physical Chemistry Chemical Physics* **2015**, *17* (36), 23521-23531, DOI: 10.1039/C5CP02008E.

(60) Keith, J. A.; Grice, K. A.; Kubiak, C. P.; Carter, E. A. Elucidation of the Selectivity of Proton-Dependent Electrocatalytic CO_2 Reduction by fac-Re(bpy)$(CO)_3$Cl. *Journal of the American Chemical Society* **2013**, *135* (42), 15823-15829. DOI: 10.1021/ja406456g.

(61) Peterson, A. A.; Nørskov, J. K. Activity Descriptors for CO_2 Electroreduction to Methane on Transition-Metal Catalysts. *The Journal of Physical Chemistry Letters* **2012**, *3* (2), 251-258. DOI: 10.1021/jz201461p.

(62) Shi, C.; Chan, K.; Yoo, J. S.; Nørskov, J. K. Barriers of Electrochemical CO_2 Reduction on Transition Metals. *Organic Process Research & Development* **2016**, *20* (8), 1424-1430. DOI: 10.1021/acs.oprd.6b00103.

(63) Matsubara, Y.; Grills, D. C.; Kuwahara, Y. Thermodynamic Aspects of Electrocatalytic CO_2 Reduction in Acetonitrile and with an Ionic Liquid as Solvent or Electrolyte. *ACS Catalysis* **2015**, *5* (11), 6440-6452. DOI: 10.1021/acscatal.5b00656.

(64) Quan, M.; Sanchez, D.; Wasylkiw, M. F.; Smith, D. K. Voltammetry of Quinones in Unbuffered Aqueous Solution: Reassessing the Roles of Proton Transfer and Hydrogen Bonding in the Aqueous Electrochemistry of Quinones. *Journal of the American Chemical Society* **2007**, *129* (42), 12847-12856. DOI: 10.1021/ja0743083.

(65) Batchelor-McAuley, C.; Kozub, B. R.; Menshykau, D.; Compton, R. G. Voltammetric Responses of Surface-Bound and Solution-Phase Anthraquinone Moieties in the Presence of Unbuffered Aqueous Media. *The Journal of Physical Chemistry C* **2011**, *115* (3), 714-718. DOI: 10.1021/jp1096585.

(66) García Rey, N.; Dlott, D. D. Effects of water on low-overpotential CO_2 reduction in ionic liquid studied by sum-frequency generation spectroscopy. *Physical Chemistry Chemical Physics* **2017**, *19* (16), 10491-10501, DOI: 10.1039/C7CP00118E.

(67) Ohio Supercomputer Center. 1987. https://www.osc.edu/about/mission (accessed 2024-08-06)

TOC Graphic

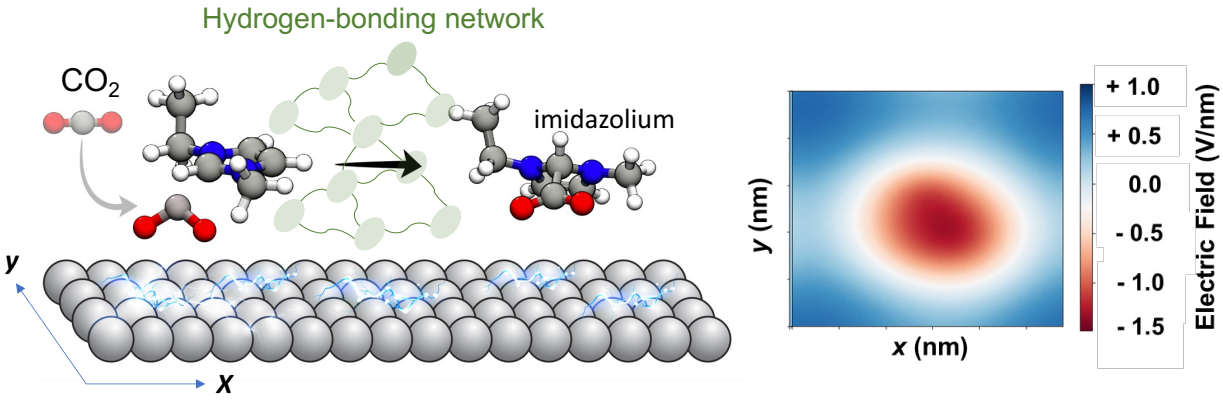
Hydrogen-bonding network
CO_2
imidazolium
y
X
y (nm)
x (nm)
+ 1.0
+ 0.5
0.0
- 0.5
- 1.0
- 1.5
Electric Field (V/nm)